Guided Ion Beam and Ab Initio Studies of Platinum Chloride Cations

R. Liyanage, M. L. Styles, R. A. J. O'Hair, and P. B. Armentrout*

Department of Chemistry, University of Utah, Salt Lake City, Utah 84112, and Contribution from the School of Chemistry, University of Melbourne, VIC 3010 Australia

Received: August 2, 2003; In Final Form: September 25, 2003

The reactions of Pt^+ and $PtCl^+$ with Cl_2, ligand exchange reactions of $PtCl^+$ and $PtCl_2^+$ with CO, and collision-induced dissociation (CID) of $PtCl^+$, $PtCl_2^+$, and $PtClCO^+$ are studied in a guided ion beam tandem mass spectrometer. The reactions with Cl_2 are exothermic and efficient at thermal energies, producing $PtCl^+$ and $PtCl_2^+$, respectively. The ligand exchange reactions of $PtCl^+$ yield $PtCO^+$ and of $PtCl_2^+$ produce $PtClCO^+$ and $PtCO^+$, all in endothermic processes. In addition, $PtCl_2^+$ reacts with CO to form C−Cl bonds yielding both Cl_2CO and ClCO. The kinetic energy dependence of these reactions and of the CID processes are analyzed to yield bond dissociation energies (BDEs) at 0 K for Pt^+−Cl and $ClPt^+$−Cl, 2.55 ± 0.15 and 2.67 ± 0.19 eV, respectively, along with BDEs for Cl−CO of 0.74 ± 0.20 eV and for Cl−COCl of 2.82 ± 0.20 eV. The structures and energetics of the $PtCl^+$ and $PtCl_2^+$ molecules and the potential energy surface for the reaction of Pt^+ with Cl_2 are calculated using density functional theory.

Introduction

In a recent study, we examined the sequential bond energies for dissociation of $Pt^+(NH_3)_x$ ($x = 1-4$) complexes using guided ion beam mass spectrometry and complemented this experimental work with density functional theory (DFT) calculations that investigated the structures and energetics of these complexes.[1] This study was designed as a first step to experimentally probe *unsaturated* platinum species that could potentially be key intermediates or active agents in reaction pathways for the activation of C−H bonds in alkanes[2−5] and of important biological mechanisms.[6−16] In particular, the platinum ammonia ligand system forms part of a model for the square planar cisplatin complex, *cis*-$Pt(NH_3)_2Cl_2$, which is not only used in the treatment of cancer but has recently been shown to catalyze the oxidation of methane to methanol.[3−5] Cisplatin is one of several $Pt(L)_xCl_y$ species ($x = 1-3$, $y = 1, 2$), where L is a nitrogen-based ligand, that have proven to be of biological importance.[7−9,17−25] Gas-phase studies of cisplatin and cisplatin analogues have generally been limited to mass spectrometric techniques that analyze whether the platinum adducts bind to various proteins or DNA,[26−32] although a recent study has used electrospray ionization and multistage mass spectrometry experiments to examine the hydrolysis products of cisplatin.[33] Previous work showed that the collision-induced dissociation (CID) reactions of $[Pt(L_3)M]^{2+}$ and $[Pt(L_3)(M-H)]^+$ (L_3 = 2,2′:6′,2″-terpyridine, diethylenetriamine, and triammonium $(NH_3)_3$; M = amino acid derivatives and simple peptides) are dependent on the nature of L_3, M, and the charge state of the ion.[34,35] Recent matrix isolation studies have observed and spectroscopically characterized PtCl and $PtCl_2$ for the first time.[36] Despite the many studies conducted in both condensed and gas phases, our study of the $Pt^+(NH_3)_x$ complexes provides some of the first thermodynamic information about simple model systems of $Pt(NH_3)_xCl_y$ complexes.

In the present work, we elucidate thermochemistry for the other component of the cisplatin ligand sequence, namely, platinum chlorine bonds. Reactions of Pt^+ and $PtCl^+$ with Cl_2 are examined and found to produce $PtCl^+$ and $PtCl_2^+$ in exothermic reactions, providing limits to the desired thermochemistry. Collision-induced dissociation (CID) of these platinum chloride ions is also examined to yield more direct measures of the bond energies. Verification of this thermochemistry is provided by examining ligand exchange reactions of $PtCl^+$ and $PtCl_2^+$ with CO, which relies on our previously determined Pt^+−CO bond energy.[37,38] To help elucidate the nature of the platinum chloride ions, we also conducted density functional theory (DFT) calculations on these species including a full potential surface for the interaction of Pt^+ with Cl_2. To complete our gas-phase examination of models for cisplatin, studies of the various $Pt^+(NH_3)_xCl_y$ species are in progress.

Experimental and Computational Section

Ion Source. Reactions are studied using a guided ion beam tandem mass spectrometer that has been described in detail elsewhere.[39,40] Pt^+ ions were generated in a continuous dc discharge by sputtering of an iron cathode with a cavity containing platinum metal. Typical operating conditions of the discharge are 1−2.5 kV and 20−30 mA in a flow of approximately 10% argon in helium. $PtCl^+$ and $PtCl_2^+$ are formed by reaction of Pt^+ with Cl_2 introduced about 50 cm downstream in the flow tube. As shown below, Pt^+ reacts efficiently with Cl_2 under single collisions conditions to form $PtCl^+$. Under multiple collision conditions, the $PtCl^+$ ion is rapidly converted to $PtCl_2^+$. Hence, both mono- and di- chloro platinum cations are easily generated by leaking controlled amounts of Cl_2 into the flow tube. Other sources of chlorine were also investigated. Reactions of carbon tetrachloride with Pt^+ resulted in large abundances of $[Pt,C,Cl]^+$ ions being formed. Donation of a chlorine atom from chloroform, dichloromethane, benzyl chloride, and methyl chloride should be energetically unfavorable.[41] We also attempted to form $PtCl^+$ ions by using $PtCl_2$ powder in the dc discharge cavity, but this failed to generate sufficient intensities of $PtCl^+$ ions. To form $PtClCO^+$, CO was introduced into the flow tube along with Cl_2.

* To whom correspondence should be addressed.

10.1021/jp036265s CCC: $25.00
Published on Web 11/06/2003

The flow conditions used in this ion source provide in excess of 10^4 collisions between an ion and the buffer gas, which should thermalize the ions both vibrationally and rotationally. However, trace amounts of low-lying excited states of Pt^+ are observed to survive these flow conditions, as found by examining the test reaction of Pt^+ with O_2.[38] These excited species are easily removed by introducing O_2 to the flow tube about 15 cm downstream of the discharge zone at a pressure of ~150 mTorr. With the addition of such a cooling gas, the DC/FT source produces metal ions in the ground state. For example, on the basis of comparisons to a surface ionization source, the DC/FT source was found to generate Sc^+,[42] Fe^+,[43] Co^+,[44] Ni^+,[45] Ru^+,[46] Rh^+,[46] and Pd^+ [46] ions with an average electronic temperature of 700 ± 400 K, and Y^+, Zr^+, Nb^+, and Mo^+ ions with an average electronic temperature of 300 ± 100 K.[47] Therefore, Pt^+ ions created under such conditions are believed to be in the ground $^2D_{5/2}(5d^9)$ electronic state term. Even at 1100 K, the population of the lowest-lying excited electronic term, $^4F_{9/2}$ at 0.593 eV,[48] is only 0.3%, such that 99.7% of the ions are in the $^2D_{5/2}$ ground state. Thus, the average electronic energy at this temperature is only 0.002 eV. This is consistent with the failure to observe any evidence for electronically excited Pt^+ species in the present or related studies[38,49] once the O_2 cooling gas is added to the flow tube.

Experimental Procedures. The $PtCl_x^+$ ions are extracted from the source, accelerated, and focused into a magnetic sector momentum analyzer for mass analysis. Mass selected ions are decelerated to a desired kinetic energy and focused into a radio frequency octopole ion guide, which traps the ions in the radial direction.[50,51] The octopole passes through a static gas cell containing Cl_2, CO, or Xe at relatively low pressures (0.04−0.2 mTorr). Product and unreacted beam ions drift to the end of the octopole, where they are focused into a quadrupole mass filter for mass analysis and detected by a secondary electron scintillation detector using standard pulse counting techniques. Ion intensities are converted into absolute cross sections as described previously.[50] Absolute uncertainties in cross section magnitudes are estimated to be ±20%, which is largely the result of uncertainties in the pressure measurement and the length of the interaction region. Relative uncertainties are approximately ±5%.

Ion kinetic energies in the laboratory frame of reference, E_{lab}, are converted to energies in the center-of-mass frame, E_{cm}, using the formula $E_{cm} = E_{lab}m/(m + M)$ where M and m are the masses of the ionic and neutral reactants, respectively. All energies reported below are in the center-of-mass frame unless otherwise specified. The absolute zero and distribution of the ion kinetic energies are determined using the octopole ion guide as a retarding potential analyzer, as previously described.[50] The distribution of the ion kinetic energies is nearly Gaussian, with a fwhm typically between 0.5 and 0.7 eV (lab) for these experiments. The uncertainty in the absolute energy scale is ±0.05 eV (lab).

Pressure dependent studies were performed on all cross sections to determine the presence and magnitude of any effects resulting from multiple collisions that may influence the shape of the cross sections.[52] In the current systems, there is an obvious pressure dependence in the $Pt^+ + Cl_2$ system, that is described below. For the two CID processes, we observe small cross sections at low energies that have an obvious pressure dependence. We attribute this to multiple energizing collisions that lead to an enhanced probability of dissociation at energies below the threshold. Data free from pressure effects is obtained by extrapolating to zero reactant pressure, as described previously.[52] Thus, data reported below result from single bimolecular collisions exclusively, unless noted otherwise.

Computational Procedures. Density functional calculations (DFT)[53,54] based on the hybrid gradient-corrected exchange functional proposed by Becke[55] combined with the gradient-corrected correlation functional of Lee, Yang, and Parr,[56] commonly known as B3LYP functional, were carried out with the Gaussian 98 suite of programs.[57] The DFT method based on the hybrid B3LYP functional has been shown to be a better approach to model binding energies of transition metal atoms compared to classical HF methods.[55] Scott and Radom[58] have shown that B3LYP harmonic vibrational frequencies reproduce observed fundamentals with good accuracy. In this work, the 60 core electrons of platinum are described by the VDZ (n + 1) relativistic effective core potential (RECP) of Hay-Wadt (HW),[59] equivalent to the Los Alamos double-ζ ECP (LANL2DZ) basis set. The HW-ECP is optimized for neutral atoms, whereas the positive charge differentially contracts the s orbitals compared to the d orbitals. Hence, calculations were performed with an altered HW-ECP basis for Pt^+ as described by Ohanessian et al. (HW+).[60] On chlorine, most calculations used the 6-311+G(3df) basis. Full geometry optimizations were performed using this hybrid basis set, which, for convenience, we will refer to as HW+/6-311+G(3df). Vibrational analyses at this level were performed on all optimized geometries to verify that they represent minima on the potential energy surface. Vibrational frequencies and rotational constants obtained were used for thermochemical analysis of the experimental cross sections as detailed in the following section. Zero-point energy corrections to the theoretical energies used these vibrational frequencies scaled by 0.989.[61] For comparison, calculations of geometries and energies were also performed using the Stuttgart−Dresden (SD) ECP for platinum.[62] Here, geometries were optimized at the B3LYP/SD/6-31G* level followed by single-point calculations at the B3LYP/SD/6-311+G(3df) level. We also performed a scan of the potential energy surface for the interaction of Pt^+ with Cl_2 at a somewhat lower level of theory, B3LYP using a 6-31+G* basis on Cl and the HW+ basis on Pt^+.

Thermochemical Analysis. Threshold regions of the reaction cross sections are modeled using eq 1

$$\sigma(E) = \sigma_0 \sum g_i(E + E_i - E_0)^n/E \qquad (1)$$

where σ_0 is an energy independent scaling factor, E is the relative translational energy of the reactants, E_0 is the energy threshold for reaction of the ground electronic and rovibrational state, and n is an adjustable parameter. The summation is over the rovibrational states of the reactant ions, i, where E_i is the excitation energy of each state and g_i is the population of those states ($\sum g_i = 1$). In our analysis of the data, we have made the assumption that the ions produced in this source are in their electronic ground states with internal energies that are well described by a Maxwell−Boltzmann distribution of rovibrational states at 300 K. Previous work from this laboratory has shown that similar assumptions are generally valid.[63−68] The assumption that products formed at threshold have an internal temperature of 0 K has been described and tested in detail previously.[69] Treating all of the energy of the ion, vibrational, rotational, and translational, as capable of coupling to the dissociation coordinate has been shown to lead to reasonable thermochemistry. The threshold energies for dissociation reactions, as determined by analysis with eq 1, are converted to bond dissociation energies (BDEs) by assuming that E_0 represents the energy difference between reactants and products. This requires that

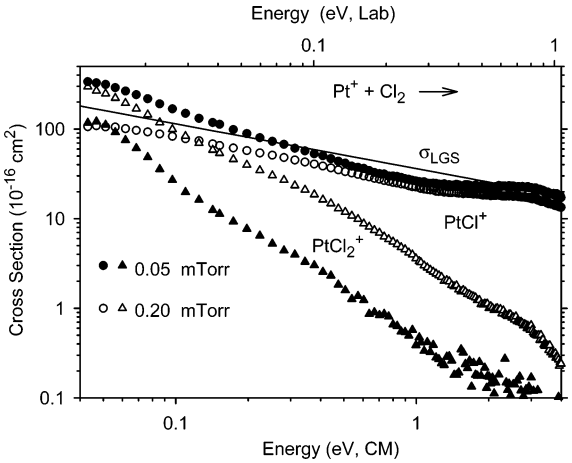

Figure 1. Cross sections for reaction of Pt^+ with Cl_2 as a function of kinetic energy in the center-of-mass frame (lower *x* axis) and the laboratory frame (upper *x* axis). Results are shown for two pressures of Cl_2: 0.05 mTorr (solid symbols) and 0.2 mTorr (open symbols). The line shows the LGS collision cross section.

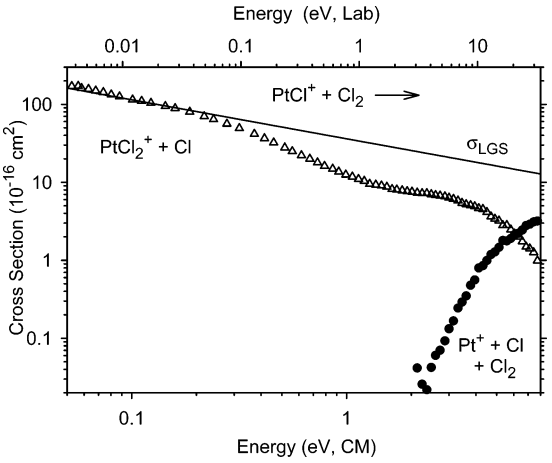

Figure 2. Cross sections for reaction of $PtCl^+$ with Cl_2 as a function of kinetic energy in the center-of-mass frame (lower *x* axis) and the laboratory frame (upper *x* axis). The line shows the LGS collision cross section.

there are no reverse activation barriers in excess of the endothermicity of dissociation, which is often true for ion−molecule reactions because of the long-range ion-induced dipole and higher order interactions.[70] Because all sources of reactant energy are included in the threshold analysis, the BDEs so determined correspond to the thermodynamic values at 0 K.

In some cases, a modification of eq 1 that includes statistical modeling of two parallel competitive dissociation pathways is used to reproduce the data. This uses equations that are provided in detail elsewhere.[71] This procedure allows more accurate modeling of the higher energy threshold of the two pathways, as it explicitly accounts for the competition between the two channels.

Results

In all systems described below, the cross sections have been corrected for the chlorine isotopes such that the cross sections are representative of the total amounts of the chemical species shown.

Pt^+ and $PtCl^+ + Cl_2$. Cross sections for the reaction of Pt^+ with Cl_2 are shown in Figure 1. It can be seen that the reaction forms both $PtCl^+$ and $PtCl_2^+$ but that the ratios of these products are strongly dependent on the pressure of the Cl_2 reactant. At low Cl_2 pressures, the cross section for formation of $PtCl^+$ is comparable to the collision cross section, as estimated from the Langevin−Gioumousis−Stevenson (LGS) model for ion-induced dipole interactions.[72] This shows that the primary process is reaction 2

$$Pt^+ + Cl_2 \rightarrow PtCl^+ + Cl \qquad (2)$$

Deviations from the LGS model at low energies can probably be attributed to small uncertainties in the absolute zero of energy (<0.02 eV lab) and to the complexities of the multiple collision processes occurring. As the pressure is raised, the $PtCl^+$ product is depleted by a secondary reaction to form $PtCl_2^+$, reaction 3, which can dominate at low energies

$$PtCl^+ + Cl_2 \rightarrow PtCl_2^+ + Cl \qquad (3)$$

The energy dependence of these cross sections indicates that both the primary and secondary reactions are exothermic and exhibit no barriers in excess of the asymptotic energy of the reactants. This indicates that the Pt^+−Cl and $ClPt^+$−Cl bond energies exceed that of Cl−Cl, 2.48 eV.[41]

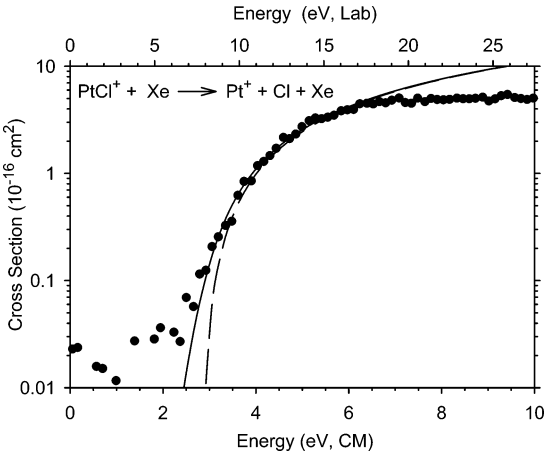

Figure 3. Cross sections for collision-induced dissociation of $PtCl^+$ by Xe as a function of kinetic energy in the center-of-mass frame (lower *x* axis) and the laboratory frame (upper *x* axis). The solid line shows the model of eq 1 convoluted over the internal and kinetic energy distributions of the reactants. The dashed line shows the model cross section for monoenergetic collisions with reactants at 0 K internal energy.

To check the exothermicity of the secondary process, the reaction of $PtCl^+$ with Cl_2 was examined independently. The results, shown in Figure 2, verify that the formation of $PtCl_2^+$ in reaction 3 is efficient and exothermic. Comparison to the LGS collision cross section shows that the process occurs on every collision. At high energies, a Pt^+ product formed in reaction 4 is also observed. As will be seen in the next section, the energy dependence of this process is consistent with the simple collision-induced dissociation (CID) reaction

$$PtCl^+ + Cl_2 \rightarrow Pt^+ + Cl + Cl_2 \qquad (4)$$

CID of $PtCl^+$ and $PtCl_2^+$. To further characterize the platinum chloride cations, we examined the collision-induced dissociation of the $PtCl^+$ and $PtCl_2^+$ ions with Xe, as shown in Figures 3 and 4. $PtCl^+$ dissociates exclusively by loss of a chlorine atom, whereas $PtCl_2^+$ is observed to lose both a chlorine atom and a chlorine molecule yielding $PtCl^+$ and Pt^+, respectively. Direct comparison of the CID processes for Cl atom loss in the two systems indicates that the dissociation of $PtCl_2^+$ is

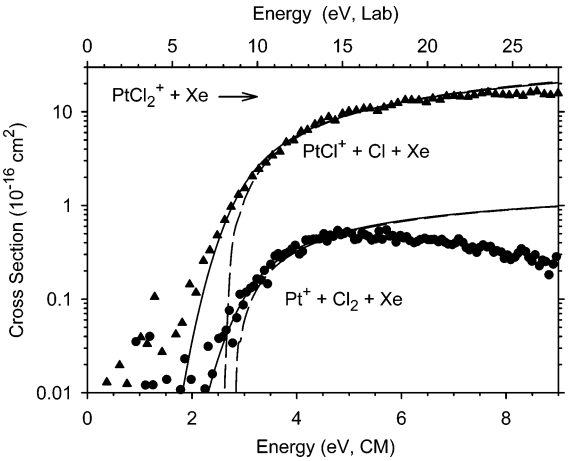

Figure 4. Cross sections for collision-induced dissociation of $PtCl_2^+$ by Xe as a function of kinetic energy in the center-of-mass frame (lower *x* axis) and the laboratory frame (upper *x* axis). The solid lines show the models of eq 1 convoluted over the internal and kinetic energy distributions of the reactants. The dashed lines show the model cross sections for monoenergetic collisions with reactants at 0 K internal energy.

TABLE 1: Optimized Parameters of eq 1 in the Analysis of Reactions with Cl_2 and CID Processes

reactant	products	σ_0, 10^{-16} cm^2 eV^{1-n}	n	E_0, eV
$Pt^+ + Cl_2$	$PtCl^+ + Cl$			<0
$PtCl^+ + Cl_2$	$PtCl_2^+ + Cl$			<0
$PtCl^+ + Xe$	$Pt^+ + Cl + Xe$	2.9 ± 0.8	1.8 ± 0.4	2.84 ± 0.25
$PtCl_2^+ + Xe$	$PtCl^+ + Cl + Xe$	13.2 ± 1.8	1.4 ± 0.2	2.61 ± 0.21
	$Pt^+ + Cl_2 + Xe$	1.0 ± 0.1	1.2 ± 0.1	2.77 ± 0.08
$PtCl^+ + CO$	$PtCO^+ + Cl$	0.6 ± 0.1	1.1 ± 0.1	0.22 ± 0.03
	$Pt^+ + Cl + CO$	1.7 ± 0.3	1.4 ± 0.1	2.69 ± 0.23
$PtCl_2^+ + CO$	$PtCO^+ + Cl_2$	0.5 ± 0.1	1.5 ± 0.2	0.56 ± 0.09
	$PtClCO^+ + Cl$	0.6 ± 0.1	1.2 ± 0.2	0.85 ± 0.15
	$Pt^+ + Cl_2CO$	~ 0.06	1.0	~ 2.0
	$PtCl^+ + ClCO$	1.2 ± 0.2	1.8 ± 0.1	1.93 ± 0.07
$PtClCO^+ + Xe$	$PtCl^+ + CO + Xe$	14.0 ± 1.9	1.2 ± 0.2	1.73 ± 0.16
	$PtCO^+ + Cl + Xe$	137 ± 18	1.2 ± 0.2	1.99 ± 0.12[a]
	$Pt^+ + CO + Cl + Xe$	0.6 ± 0.3	1.2 ± 0.2	4.25 ± 0.30

[a] The competition with $PtCl^+$ was explicitly included in the analysis of these data.

more efficient and has a lower threshold than for $PtCl^+$. Also the observation that Cl_2 elimination from $PtCl_2^+$ is more endothermic than Cl elimination is consistent with the fact that $D(Pt^+-Cl) > D(Cl-Cl)$. In these systems, we did not observe any appreciable amounts of the ligand exchange products, $Pt^+(Xe)$ or $PtCl^+(Xe)$.

Analyses of these CID cross sections with eq 1 yields the optimum fitting parameters given in Table 1. Modeling of these cross sections reproduces the cross sections over extended ranges of energy and magnitude, as shown in Figures 3 and 4. The thresholds for Cl atom loss obtained are 2.84 ± 0.25 eV for $PtCl^+$ and 2.61 ± 0.21 eV for $PtCl_2^+$. If these thresholds are equated with the bond dissociation energies of these species, we find that the results agree with the lower limit of 2.48 eV, determined from reactions 2 and 3. However, CID of small covalently bound species with strong bonds is sometimes limited by the efficiency of energy transfer, rather than the thermodynamic threshold.[73-75] In such cases, the CID threshold is only an upper limit to the true bond energy.

Alternatively, we can use the threshold for the elimination of molecular chlorine to narrow the thermodynamic possibilities. We measure that $PtCl_2^+ \rightarrow Pt^+ + Cl_2$ requires 2.77 ± 0.08 eV, which means that $D(Pt^+-Cl) + D(ClPt^+-Cl) = D(Pt^+-Cl_2) + D(Cl_2) = 5.25 \pm 0.08$ eV. This agrees with the bond energy sum of $2.84 + 2.61 = 5.45 \pm 0.33$ eV derived from the Cl atom loss thresholds.

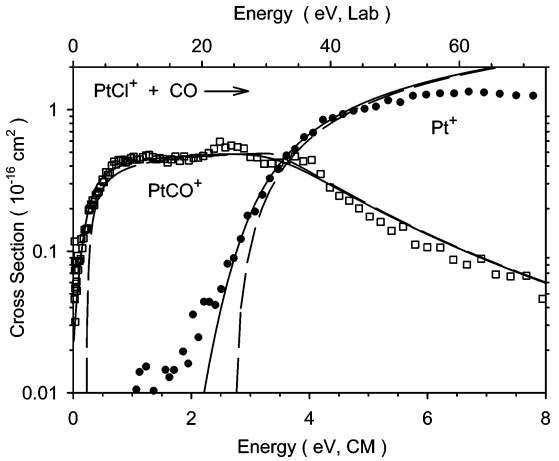

Figure 5. Cross sections for reaction of $PtCl^+$ with CO as a function of kinetic energy in the center-of-mass frame (lower *x* axis) and the laboratory frame (upper *x* axis). The solid lines show the models of eq 1 convoluted over the internal and kinetic energy distributions of the reactants. The dashed lines show the model cross sections for monoenergetic collisions with reactants at 0 K internal energy.

Ligand Exchange Reactions. An alternative way of characterizing the $PtCl_x^+$ species is to react them with a reagent that will displace the Cl ligand. Our choice for this study was CO, for which we have measured the Pt^+-CO bond energy in two separate ways,[37,38] as discussed in detail below. Reaction of $PtCl^+$ with CO, shown in Figure 5, yields two products formed in a ligand exchange process, reaction 5, and simple CID, reaction 6

$$PtCl^+ + CO \rightarrow PtCO^+ + Cl \quad (5)$$

$$\rightarrow Pt^+ + Cl + CO \quad (6)$$

The dominant reaction is the ligand exchange process, which appears to be slightly endothermic (although there is an exothermic tail indicating the thermalization of the $PtCl^+$ ions is incomplete). Analysis of these data provides a threshold of 0.22 ± 0.03 eV (Table 1), which is just the difference between $D(Pt^+-CO)$ and $D(Pt^+-Cl)$, as discussed further below. At higher energies, this cross section declines as that for the CID process 5 increases, consistent with sequential or competitive processes. (The structure observed in the $PtCO^+$ cross section between 2 and 3 eV in this figure is not reproducible.) The threshold measured for the CID process is comparable to that obtained with the Xe collision gas, Table 1.

Reaction of $PtCl_2^+$ with CO is more complex, resulting in four different processes, reactions 7-10, as shown in Figure 6.

$$PtCl_2^+ + CO \rightarrow PtCO^+ + Cl_2 \quad (7)$$

$$\rightarrow PtCl(CO)^+ + Cl \quad (8)$$

$$\rightarrow PtCl^+ + ClCO \quad (9)$$

$$\rightarrow Pt^+ + Cl_2CO \quad (10)$$

Reactions 7 and 8 both have similarly low thresholds, not unlike the relative thresholds for loss of Cl and Cl_2 from $PtCl_2^+$ in the Xe system. The threshold for formation of $PtCl^+$, measured as 1.93 ± 0.07 eV, is 0.68 ± 0.22 eV below that observed for the generation of this ion in the Xe collision system.

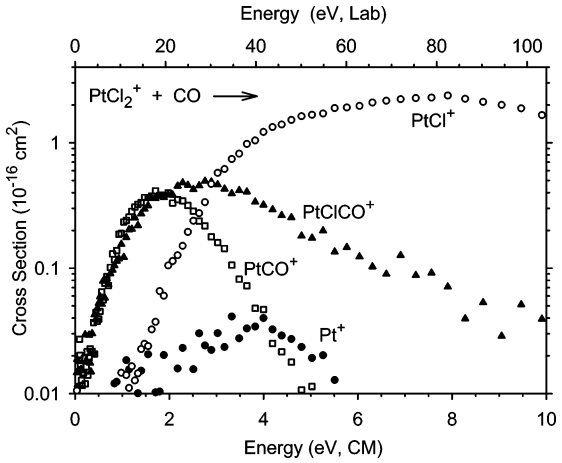

Figure 6. Cross sections for reaction of $PtCl_2^+$ with CO as a function of kinetic energy in the center-of-mass frame (lower *x* axis) and the laboratory frame (upper *x* axis). Because of the complexity of the results, model cross sections are not shown.

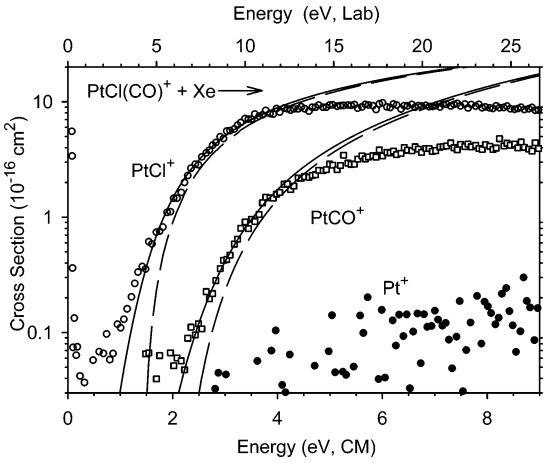

Figure 7. Cross sections for collision-induced dissociation of $PtCl(CO)^+$ by Xe as a function of kinetic energy in the center-of-mass frame (lower *x* axis) and the laboratory frame (upper *x* axis). The solid lines show the models of eq 1 convoluted over the internal and kinetic energy distributions of the reactants. The dashed lines show the model cross sections for monoenergetic collisions with reactants at 0 K internal energy.

This indicates that the neutral products must be the ClCO radical rather than separated Cl and CO. This is consistent with an estimate of the Cl−CO bond energy of 0.73 ± 0.44 eV in the literature.[76] (By examining the sequential bond energies for removing methyl groups from acetone, the JANAF tables estimate that the Cl−COCl bond energy is four times that for Cl−CO.) The cross section for Pt^+ formation has an apparent threshold well below that for the loss of Cl_2 from $PtCl_2^+$ in the Xe system. This indicates that the neutral product must be Cl_2CO, which is 1.03 eV lower in energy than Cl_2 + CO.[76] Given the threshold determined above for $D(Pt^+-Cl_2)$, reaction 10 should occur beginning about 1.7 eV, in rough agreement with the data. Unfortunately, the Pt^+ cross section is sufficiently small and scattered that analysis of this cross section is not definitive; hence, only a simple estimate (use of eq 1 with *n* held to unity) is provided in Table 1. A slightly higher value of *n* would give a threshold consistent with 1.7 eV and provide a better reproduction of the data.

CID of $PtCl(CO)^+$. To characterize one of the products observed in the reaction of $PtCl_2^+$ with CO more thoroughly, the $PtCl(CO)^+$ species was generated in the flow tube and activated by collisions with Xe. As shown in Figure 7, two major processes are observed as reactions 11 and 12, with reaction 13 being a small, high energy process

$$PtCl(CO)^+ + Xe \rightarrow PtCl^+ + CO + Xe \quad (11)$$

$$\rightarrow PtCO^+ + Cl + Xe \quad (12)$$

$$\rightarrow Pt^+ + Cl + CO \quad (13)$$

The relative thresholds observed for reactions 11 and 12 provide direct evidence that the $PtCl^+$ bond is stronger than the $PtCO^+$ bond, in agreement with the endothermic ligand exchange process, reaction 5. Indeed, analysis of the cross sections for reactions 11 and 12 using a model that accounts for competition provides a relative threshold of 0.27 ± 0.05 eV, in good agreement with the endothermicity measured for reaction 5, Table 1. (The precision of the relative threshold determination is better than the absolute thresholds listed in Table 1 because many systematic errors cancel.) It might be noted that a rather large relative scaling factor of 9.9 ± 1.4 was needed to adequately reproduce the magnitude of reaction 12. The different electronic degeneracies of the products, $g = 3$ for reaction 11 and $g = 12$ for reaction 12, may contribute to the difference in magnitudes between the two channels, but even this does not fully account for observed scaling factor. Further, it can be seen that there is an exothermic feature in the $PtCl^+$ cross section, demonstrating that the $PtCl(CO)^+$ species is not fully thermalized. Such hot ions are also believed to prevent fitting of the threshold region of the $PtCl^+$ cross section with high fidelity, Figure 7.

TABLE 2: Theoretical Geometries for $PtCl_x^+$ Species

structure	state	r(Pt^+−Cl)	r(Cl−Cl)	∠ClPtCl
Cl_2	$^1\Sigma_g^+$		2.011, *2.045*	
Pt^+−Cl	$^1\Sigma^+$	2.136, *2.159*		
	$^3\Sigma^-$	2.135, *2.156*		
ClPt$^+$−Cl	$^2A_2$	2.148, 2.148	3.691	118.5
		2.166, *2.166*	*3.665*	*115.6*
ClPt$^+$−Cl (linear)	$^2\Pi_g$	2.126, 2.126	4.251	180.0
		2.144, *2.144*	*4.289*	*180.0*
Pt^+−Cl_2	$^2A''$	2.324, 3.564	2.022	32.5
		2.374, *3.641*	*2.066*	*32.2*
TS (Pt^+−Cl_2)	$^2A''$	2.336, 2.624	2.247	53.5

[a] Bond lengths are in angstroms, and bond angles are in degrees. B3LYP/HW+/6-311+G(3df) values. Values in italics are B3LYP/SD/6-311+G(3df)// B3LYP/SD/6-31+G*.

Computational Results. Table 2 provides the fully optimized ground-state geometries for the $PtCl^+$ and $PtCl_2^+$ structures located on the B3LYP/HW+/6-311+G(3df) and B3LYP/SD/6-311+G(3df)// B3LYP/SD/6-31+G* potential energy surfaces. Table 3 lists energies, vibrational frequencies (scaled by 0.989), and rotational constants of these systems calculated at these levels, along with adiabatic bond dissociation energies calculated from the absolute energies corrected for zero-point energies.

Both a singlet and triplet state of $PtCl^+$ were located, with nearly identical bond lengths of 2.136 and 2.135 Å, respectively. These calculations indicate that $PtCl^+(^3\Sigma^-)$ is the ground state with the $^1\Sigma^+$ being higher in energy by 1.12 eV (both HW+ and SD results). It might have been anticipated that the coupling of $Pt^+(^2D,5d^9)$ with $Cl(^2P,3p^5)$ would lead to a covalent bond formation and a singlet ground state. Indeed, the valence electronic configuration of the $^1\Sigma^+$ state is $(1\sigma)^2(1\pi)^4(1\delta)^4(2\pi^*)^4$ where the 1σ and 1π orbitals are bonding, the 1δ orbitals are metal-based nonbonding, and the $2\pi^*$ are antibonding orbitals. However, the $^3\Sigma^-$ ground state utilizes the empty 6s orbital on platinum giving a $(1\sigma)^2(1\pi)^4(1\delta)^4(2\sigma)^2(2\pi^*)^2$ configuration

TABLE 3: Theoretical Absolute Energies, Vibrational Frequencies, Rotational Constants, and Bond Dissociation Energies for $PtCl_x^+$ Species

structure	state	energy[a] (h)	ν (cm^{-1})[b]	B (cm^{-1})[c]	BDE (eV)[d]
Pt^+	^2D	−118.737255			
		−118.963601			
Cl	^2P	−460.168406			
Cl_2	$^1\Sigma_g^+$	−920.424672	535	0.238	2.358
		−920.424273			*2.347*
Pt^+-Cl	$^1\Sigma^+$	−578.956536	411	0.125	1.359
		−579.181279			*1.315*
	$^3\Sigma^-$	−578.997736	417	0.125	2.480
		−579.222382			*2.433*
$ClPt^+-Cl$	$^2A_2$	−1039.255324	64, 420, 432	0.271, 0.071, 0.056	2.396
		−1039.481130			*2.427*
$ClPt^+-Cl$ (linear)	$^2\Pi_g$	−1039.246408	−73 (2), 423, 476	0.053 (2)	2.154
		−1039.473300			*2.215*
Pt^+-Cl_2	$^2A''$	−1039.216938	107, 255, 486	0.428, 0.038, 0.035	1.478
		−1039.440710			*1.418*
TS (Pt^+-Cl_2)	$^2A''$	−1039.191628	−304, 129, 320	0.197, 0.066, 0.049	0.814

[a] B3LYP/HW+/6-311+G(3df) values. Values in italics are B3LYP/SD/6-311+G(3df)// B3LYP/SD/6-31+G*. [b] Vibrational frequencies calculated at the B3LYP/HW+/6-311+G(3df) level and scaled by 0.989. [c] Rotational constants calculated at the B3LYP/HW+/6-311+(3df) level. [d] Bond dissociation energies corrected for zero-point vibrational energies.

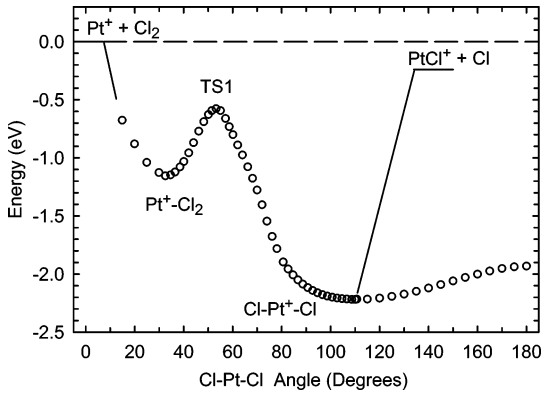

Figure 8. Calculated potential energy surface for interaction of Pt^+ with Cl_2. All calculations performed at the B3LYP/HW+/6-31+G* level.

where the 2σ orbital is a 6s−5dσ hybrid that is largely nonbonding. The movement of two electrons from antibonding to nonbonding orbitals results in the more stable triplet state.

For the platinum dichloride cation, the $^2A_2$ ground-state geometry has a Cl−Pt−Cl bond angle of 118.5° and slightly longer but equal Pt−Cl bonds, 2.148 Å. We also constrained the bond angle to 180° and found a $^2\Pi_g$ transition state with bond lengths of 2.126 Å. For $PtCl_2^+$, the linear structure is higher in energy than the cis geometry by only 0.24 (0.21 SD) eV. Another minimum located for this system is a $Pt^+(Cl_2)$ adduct, having a $^2A''$ ground state and lying 1.04 (1.10 SD) eV higher than the ground-state $PtCl_2^+$ molecule. The Pt^+-Cl bond length of 2.324 Å is long compared to the covalent bonds in $PtCl^+$ and $PtCl_2^+$. The Cl−Cl bond length in this complex is 2.022 Å, very similar to that calculated for the uncomplexed Cl_2 molecule, 2.011 Å. Clearly, the adduct can be viewed as an interaction between the highest occupied molecular orbital of Cl_2, one of the valence π^* orbitals, and the empty 6s orbital on Pt^+, which hybridizes with the singly occupied 5d orbital.

Potential Energy Surface. To more fully understand the reaction of Pt^+ with Cl_2, we also examined the potential energy surface for this interaction at a B3LYP/HW+/6-31+G* level (Figure 8). This surface smoothly connects the ground-state platinum dichloride cation with the linear transition state, and finds another transition state, TS1, for insertion of Pt^+ into the Cl_2 bond. Reaction path calculations (IRC) were performed in both directions from TS1 and were shown to connect smoothly to the Pt^+-Cl_2 adduct and the ground-state $ClPtCl^+$ molecule. An optimization of this TS at the B3LYP/HW+/6-311+G(3df) level gives a $^2A''$ state with Pt−Cl bond lengths of 2.336 and 2.624 Å and a Cl−Cl bond length of 2.247 Å. The Cl−Pt−Cl bond angle of 53.5° lies between those for the $Pt(Cl_2)^+$ adduct, 32.5°, and the ground-state $PtCl_2^+$ molecule. At this level of theory, the transition state lies 0.66 eV above the adduct, but still below the $Pt^+ + Cl_2$ asymptote by 0.81 eV.

Clearly, this potential energy surface can explain our experimental observations for reaction of $Pt^+ + Cl_2$ and for CID of $PtCl_2^+$. The bimolecular reaction 2 is observed to occur exothermically with near unit efficiency. This is consistent with the formation of the ground-state $ClPtCl^+$ ($^2A_2$) molecule, which then dissociates by the lowest energy path to $PtCl^+(^3\Sigma^-) + Cl(^2P)$ in a spin-allowed process. Further, this process is kinetically favored compared to elimination of Cl_2, which must pass over the tight transition state, TS1. For the same reasons, collisional activation of $PtCl_2^+$ leads to preferential dissociation to $PtCl^+ + Cl$, with small amounts of $Pt^+ + Cl_2$ at higher energies.

Discussion

Thermodynamic Results. Collision-induced dissociation is potentially a direct means of determining the bond dissociation energy of molecules. However, for strongly bound species having few degrees of freedom, we have found that the CID threshold can be elevated from the thermodynamic value because energy transfer at threshold may be inefficient.[73−75] (Note that such inefficiencies do not indicate that a reverse activation barrier is present on the potential energy surface). Thus, the thresholds for CID of $PtCl^+$ and $PtCl_2^+$ determined here are most conservatively viewed as upper limits to the true thermochemistry. Focusing first on $PtCl^+$, we find that CID with Xe and CO yield thresholds for dissociation of $PtCl^+$ of 2.84 ± 0.25 and 2.69 ± 0.23 eV, respectively. The relative bond energies of $PtCl^+$ and $PtCO^+$ can be acquired from the ligand exchange reaction 5 and the competitive dissociation of $PtCl(CO)^+$, reactions 11 and 12. These sets of results indicate that $D(Pt^+-Cl)$ exceeds $D(Pt^+-CO)$ by 0.22 ± 0.06 and 0.27 ± 0.10 eV (where two standard deviations are used). The Pt^+-CO bond energy has been measured as 2.20 ± 0.10 eV from CID of $PtCO^+$ with Xe[37] and as 2.28 ± 0.05 eV from the threshold for formation of $PtCO^+$ in the reaction of Pt^+ with CO_2.[38] Our best value for $D(Pt^+-CO)$ is the weighted average

of these two independent determinations, 2.26 ± 0.09 eV (where the uncertainty is two standard deviations of the mean). Combined with the two relative bond energies, this means that $D(Pt^+-Cl) = 2.48 \pm 0.11$ and 2.53 ± 0.13 eV, respectively. A weighted average of the four independent values for $D(Pt^+-Cl)$ gives 2.55 ± 0.15 eV (where the uncertainty is two standard deviations of the mean). This value seems reasonable given that the exothermicity of reaction 2 establishes a lower limit for this bond energy of 2.48 eV = $D(Cl_2)$.

Turning now to $PtCl_2^+$, we find that CID of this ion with Xe yields $D(ClPt^+-Cl) \leq 2.61 \pm 0.21$ eV. A value of 2.58 ± 0.22 eV is obtained by combining the thresholds for reactions 8 and 11. Combined with $D(Cl-CO) = 0.73 \pm 0.44$ eV, reaction 9 can also be used to determine this bond energy as 2.69 ± 0.45 eV, again consistent with the other values within the large uncertainty. Alternatively, we note that CID of $PtCl_2^+$ with Xe also provides $D(Pt^+-Cl_2) \leq 2.77 \pm 0.08$ eV. The latter value is nicely confirmed by the threshold for the ligand displacement reaction 7, 0.56 ± 0.09 eV, which gives $D(Pt^+-Cl_2) = 2.82 \pm 0.13$ eV when combined with $D(Pt^+-CO)$. From these values, we can find that $D(Pt^+-Cl_2) + D(Cl_2) = 5.25 \pm 0.08$ and 5.30 ± 0.13 eV. This bond energy sum is also equal to $D(ClPt^+-Cl) + D(Pt^+-Cl)$. If we combine these sums with $D(Pt^+-Cl) = 2.55 \pm 0.15$ eV, we obtain $D(ClPt^+-Cl) = 2.70 \pm 0.17$ and 2.75 ± 0.20 eV, which agree with the values above within experimental error. The weighted average of these five determinations for $D(ClPt^+-Cl)$ is 2.67 ± 0.19 eV (two standard deviations of the mean). The same five determinations can also be used to find a weighted average for $D(Pt^+-Cl) + D(ClPt^+-Cl)$ of 5.25 ± 0.13 eV (two standard deviations of the mean), from which $D(Pt^+-Cl_2) = 2.77 \pm 0.13$ eV can be derived. In all cases, these values correspond to 0 K bond energies.

Unfortunately, no thermodynamic information is available in the literature concerning the neutral PtCl or $PtCl_2$ molecules. Thermodynamic cycles could be used to provide additional information if either the heats of formation of the neutrals or their ionization energies were known.

Given the platinum chloride cation bond energies, we can return to the threshold for reaction 9 to determine a value for $D(Cl-CO)$ that is more precise than the estimate presently in the literature. Given $D(ClPt^+-Cl) = 2.67 \pm 0.19$ eV, the threshold for reaction 9 indicates that $D(Cl-CO) = 0.74 \pm 0.20$ eV. Combined with the heat of formation for Cl_2CO, this value can also be used to determine that $D(ClCO-Cl) = 2.82 \pm 0.20$ eV. The ratio of these bond energies is 1.0:3.8, consistent with the value of 4.0 used in the JANAF tables to estimate the heat of formation for ClCO.[76]

Theoretical Thermochemistry. For bond energies that include Pt^+ in the dissociation asymptote, the experimental BDE refers to the ground spin-orbit state at 0.0 eV, $a^2D_{5/2}$ for Pt^+.[48] In contrast, our calculations do not explicitly include spin-orbit interactions such that they are referenced to the properly weighted mean of all spin-orbit levels in the ground state term, 0.418 eV for $Pt^+(a^2D)$.[48,74] Likewise, calculations involving the energy of the Cl atom differ from the $^2P_{3/2}$ ground state by 0.036 eV. To properly compare with experimental values, all calculated bond energies involving Pt^+ and Cl should be corrected by these different asymptotic energies as well as any spin-orbit coupling energies in the molecular species, which are generally not available. One could assume that spin−orbit coupling is largely quenched for all molecular species containing platinum. Calculations have found spin−orbit splittings of 0.05 eV for PtO^+ and 0.10−0.18 eV for $PtCH_2^+$,[77] and experiments find 0.12 eV for neutral PtO.[78] Thus, correcting only for the atomic spin-orbit energies is clearly an approximation and an overestimation, but one that has provided better agreement between experiment and theory in other recent studies of platinum cation ligand bond energies[37,74] but not unambiguously in all.[38,75] Here, values ignoring and including (in parentheses) this atomic level correction are given in the discussion below and can be considered upper and lower limits to values that would include explicit spin-orbit interactions for all species.

Calculations at the B3LYP/6-311+G(3df) level for Cl_2 yield a reasonable bond energy of 2.36 (2.29 with the spin−orbit correction) eV compared to the experimental value of 2.48 eV, although about 5 (8)% too low. For the Pt^+-Cl, $ClPt^+-Cl$, and Pt^+-Cl_2 bond energies, calculations using the HW+ ECP find values of 2.48 (2.03), 2.40 (2.36), and 2.52 (2.10) eV, respectively, using the triplet ground state for the $PtCl^+$ species, whereas the use of the SD ECP yields values of 2.43 (1.98), 2.43 (2.39), and 2.51 (2.09) eV for these bonds. Thus, theory and experiment agree that it costs more energy to eliminate Cl_2 than Cl from $PtCl_2^+$ and that the Pt^+-Cl and $ClPt^+-Cl$ bonds are comparable in strength (although when the atomic spin−orbit energies are included, the latter bond energy greatly exceeds the former). However, theory underestimates the absolute values of all of these energies (especially if the spin-orbit corrections are included), as is clear by remembering that the exothermicities of reactions 2 and 3 demonstrate that $D(Pt^+-Cl)$ and $D(ClPt^+-Cl)$ must be greater than $D(Cl-Cl) = 2.48$ eV. If the theoretical HW+ (SD) values without spin-orbit corrections are empirically adjusted upwards by 5%, then the predictions are 2.60 (2.55), 2.52 (2.55), and 2.64 (2.63) eV for the Pt^+-Cl, $ClPt^+-Cl$, and Pt^+-Cl2 bond energies, in reasonable agreement with the best experimental values, 2.55 ± 0.15, 2.67 ± 0.19, and 2.77 ± 0.13 eV, respectively. Empirically, the best agreement requires an upward adjustment of 8 ± 3%. Theoretical values including the spin−orbit corrections require a much larger empirical shift to bring them into agreement with experiment, about 12% for the $ClPt^+-Cl$ bond energy and about 30% for the Pt^+-Cl and Pt^+-Cl_2 bond energies. These comparisons may suggest that the spin−orbit coupling in $PtCl^+$ and $PtCl_2^+$ is still appreciable.

Acknowledgment. M.L.S. acknowledges the award of a Melbourne University Abroad Travelling Scholarship and an APA Commonwealth Postgraduate Scholarships. This work was supported by the National Science Foundation under Grant CHE-0135517.

References and Notes

(1) Liyanage, R.; Styles, M. L.; O'Hair, R. A. J.; Armentrout, P. B. *Int. J. Mass Spectrom.* **2003**, *227*, 47−62.
(2) Shilov, A. E.; Shul'pin, G. B. *Chem. Rev.* **1997**, *97*, 2879−2932.
(3) Periana, R. A.; Taube, D. J.; Gamble, S.; Taube, H.; Satoh, T.; Fujii, H. *Science* **1998**, *280*, 560−564.
(4) Kua, J.; Xu, X.; Periana, R. A.; Goddard, W. A., III. *Organometallics* **2002**, *21*, 511−525.
(5) Xu, X.; Kua, J.; Periana, R. A.; Goddard, W. A., III. *Organometallics* **2003**, *22*, 2057−2068.
(6) Miller, K. J.; Taylor, E. R.; Basch, A.; Krauss, M.; Stevens, W. J. *Biomol. Struct. Dyn.* **1985**, *2*, 1157.
(7) Miller, S. E.; House, D. A. *Inorg. Chim. Acta* **1989**, *166*, 189.
(8) Miller, S. E.; House, D. A. *Inorg. Chim. Acta* **1989**, *161*, 131.
(9) Miller, S. E.; House, D. A. *Inorg. Chim. Acta* **1990**, *173*, 53.
(10) Carloni, P.; Andreoni, W.; Hutter, J.; Curioni, A.; Gianozzi, P.; Parrinello, M. *Chem. Phys. Lett.* **1995**, *234*, 50.
(11) Basch, A.; Krauss, M.; Stevens, W. J.; Cohen, D. *Inorg. Chem.* **1985**, *24*, 3313.
(12) Car, P.; Parrinello, M. *Phys. Rev. Lett.* **1985**, *55*, 2471.
(13) Hambley, T. W. *Inorg. Chem.* **1992**, *14*, 1.
(14) Carloni, P.; Sprik, M.; Andreoni, W. *J. Phys. Chem. B* **2000**, *104*, 823.

(15) Pavankumar, P. N. V.; Seetharamulu, P.; Yao, S.; Saxe, J. D.; Reddy, D. G.; Hausheer, F. H. *J. Comput. Chem.* **1999**, *20*, 36.
(16) Burda, J. V.; Sponer, J.; Leszczynski, J. *J. Biol. Inorg. Chem.* **2000**, *5*, 178.
(17) Bamcroft, D. P.; Lepre, C. A.; Lippard, S. J. *J. Am. Chem. Soc.* **1990**, *112*, 6860.
(18) Jennette, K. W.; Gill, T. J.; Sadownick, J. A.; Lippard, S. J. *J. Am. Chem. Soc.* **1976**, *98*, 6159.
(19) Reedijk, J. *Inorg. Chim. Acta* **1992**, *198*, 873.
(20) Reedijk, J. *Chem. Commun.* **1996**, 801.
(21) Sundquist, W. I.; Lippard, S. J. *Coord. Chem. Rev.* **1990**, *100*, 293.
(22) Wong, E.; Giandomenico, C. M. *Chem. Rev.* **1999**, *99*, 2451.
(23) Lippert, B. *Cisplatin: Chemistry and Biochemistry of a Leading Anticancer Drug*; Wiley-VCH: Weinheim, 1999; Vols. 3−6.
(24) Ehrsson, H. C.; Wallin, I. B.; Andersson, A. S.; Edlund, P. O. *Anal. Chem.* **1995**, *67*, 3608.
(25) Martin, L. B.; Schreiner, A. F.; van Breemen, R. B. *Anal. Biochem.* **1991**, *193*, 6.
(26) Xu, N.; Pasa-Tolic, L.; Smith, R. D.; Ni, S.; Thrall, B. D. *Anal. Biochem.* **1999**, *272*, 26.
(27) Tokuchi, N.; Isobe, H.; Takekawa, H.; Hanada, T.; Ishida, T.; Ogura, S.; Itoh, K.; Furudate, M.; Saito, K.; Kawakami, Y. *British J. Cancer* **1998**, *77*, 1363.
(28) Kloster, M. B. G.; Hannis, J. C.; Muddiman, D. C.; Farrell, N. *Biochemistry* **1999**, *38*, 14731.
(29) Romeo, R. *Comments Inorg. Chem.* **1990**, *11*, 21.
(30) Gibson, D.; Costello, C. E. *Eur. Mass Spectrom.* **1999**, *5*, 501.
(31) Gupta, R.; Kapur, A.; Beck, J. L.; Sheil, M. M. *Rapid Commun. Mass Spectrom.* **2001**, *15*, 2472.
(32) Beck, J. L.; Colgrave, M. L.; Ralph, S. F.; Sheil, M. M. *Mass Spectrom. Rev.* **2001**, *20*, 61.
(33) Cui, M.; Mesterc, Z. *Rapid Commun. Mass Spectrom.* **2003**, *17*, 1517−1527.
(34) Styles, M. L. Ph.D. Thesis, University of Melbourne, 2001.
(35) Styles, M. L.; O'Hair, R. A. J.; McFadyen, W. D. *Eur. Mass Spectrom.* **2001**, *7*, 69−78.
(36) Bridgeman, A. J.; Cavigliasso, G.; Harris, N.; Young, N. A. *Chem. Phys. Lett.* **2002**, *351*, 319−326.
(37) Zhang, X.-G.; Armentrout, P. B. *Organometallics* **2001**, *20*, 4266−4273.
(38) Zhang, X.-G.; Armentrout, P. B. *J. Phys. Chem. A*, accepted for publication.
(39) Loh, S. K.; Hales, D. A.; Lian, L.; Armentrout, P. B. *J. Chem. Phys.* **1989**, *90*, 5466−5485.
(40) Schultz, R. H.; Armentrout, P. B. *Int. J. Mass Spectrom. Ion Processes* **1991**, *107*, 29−48.
(41) Lias, S. G.; Bartmess, J. E.; Liebman, J. F.; Holmes, J. L.; Levin, R. D.; Mallard, W. G. *J. Phys. Chem. Ref. Data Suppl. 1* **1988**, *17*, 1.
(42) Kickel, B. L.; Armentrout, P. B. *J. Am. Chem. Soc.* **1995**, *117*, 7, 4057−4070.
(43) Clemmer, D. E.; Chen, Y.-M.; Khan, F. A.; Armentrout, P. B. *J. Phys. Chem.* **1994**, *98*, 6522−6529.
(44) Haynes, C. L.; Armentrout, P. B. *Organometallics* **1994**, *13*, 3480−3490.
(45) Kickel, B. L.; Armentrout, P. B. *J. Am. Chem. Soc.* **1995**, *117*, 764−773.
(46) Chen, Y.-M.; Elkind, J. L.; Armentrout, P. B. *J. Phys. Chem.* **1995**, *99*, 10438−10445.
(47) Sievers, M. R.; Chen, Y.-M.; Elkind, J. L.; Armentrout, P. B. *J. Phys. Chem.* **1996**, *100*, 54−62.
(48) Moore, C. E. *NSRDS−NBS* **1971**, *35 (Vol. III)*, 1.
(49) Zhang, X.-G.; Armentrout, P. B. *J. Chem. Phys.* **2002**, *116*, 5565−5573.
(50) Ervin, K. M.; Armentrout, P. B. *J. Chem. Phys.* **1985**, *83*, 166−189.
(51) Gerlich, D. *Adv. Chem. Phys.* **1992**, *82*, 1−176.
(52) Hales, D. A.; Lian, L.; Armentrout, P. B. *Int. J. Mass Spectrom. Ion Processes* **1990**, *102*, 269−301.
(53) Salahub, D. R. In *Advances in Chemical Physics*; Lawley, K. P., Ed.; Wiley: New York, 1987; Vol. LXIX, p 447.
(54) Parr, R. G.; Yang, W. *Density-Functional Theory of Atoms and Molecules*; Oxford University Press: New York, 1989.
(55) Becke, A. D. *J. Chem. Phys.* **1993**, *98*, 5648−5652.
(56) Lee, C.; Yang, W.; Parr, R. G. *Phys. Rev. B* **1988**, *37*, 785−789.
(57) Frisch, M. J.; Trucks, G. W.; Schlegel, H. B.; Scuseria, G. E.; Robb, M. A.; Cheeseman, J. R.; Zakrzewski, V. G.; Montgomery, J. A., Jr.; Stratmann, R. E.; Burant, J. C.; Dapprich, S.; Millam, J. M.; Daniels, A. D.; Kudin, K. N.; Strain, M. C.; Farkas, O.; Tomasi, J.; Barone, V.; Cossi, M.; Cammi, R.; Mennucci, B.; Pomelli, C.; Adamo, C.; Clifford, S.; Ochterski, J.; Petersson, G. A.; Ayala, P. Y.; Cui, Q.; Morokuma, K.; Malick, D. K.; Rabuck, A. D.; Raghavachari, K.; Foresman, J. B.; Cioslowski, J.; Ortiz, J. V.; Stefanov, B. B.; Liu, G.; Liashenko, A.; Piskorz, P.; Komaromi, I.; Gomperts, R.; Martin, R. L.; Fox, D. J.; Keith, T.; Al-Laham, M. A.; Peng, C. Y.; Nanayakkara, A.; Gonzalez, C.; Challacombe, M.; Gill, P. M. W.; Johnson, B. G.; Chen, W.; Wong, M. W.; Andres, J. L.; Head-Gordon, M.; Replogle, E. S.; Pople, J. A. *Gaussian 98*, revision A.7; Gaussian, Inc.: Pittsburgh, PA, 1998.
(58) Scott, A. P.; Radom, L. *J. Phys. Chem.* **1996**, *100*, 16502.
(59) Hay, P. J.; Wadt, W. R. *J. Chem. Phys.* **1985**, *82*, 299−310.
(60) Ohanessian, G.; Brusich, M. J.; Goddard, W. A., III. *J. Am. Chem. Soc.* **1990**, *112*, 7179−7189.
(61) Foresman, J. B.; Frisch, A. E. *Exploring Chemistry with Electronic Structure Methods*, 2nd ed.; Gaussian, Inc.: Pittsburgh, PA, 1996.
(62) Andrae, D.; Haeussermann, U.; Dolg, M.; Stoll, H.; Preuss, H. *Theor. Chim. Acta* **1990**, *77*, 123−141.
(63) Dalleska, N. F.; Honma, K.; Armentrout, P. B. *J. Am. Chem. Soc.* **1993**, *115*, 12125−12131.
(64) Dalleska, N. F.; Honma, K.; Sunderlin, L. S.; Armentrout, P. B. *J. Am. Chem. Soc.* **1994**, *116*, 3519−3528.
(65) Khan, F. A.; Clemmer, D. E.; Schultz, R. H.; Armentrout, P. B. *J. Phys. Chem.* **1993**, *97*, 7978−7987.
(66) Schultz, R. H.; Armentrout, P. B. *J. Chem. Phys.* **1992**, *96*, 1046−1052.
(67) Fisher, E. R.; Kickel, B. L.; Armentrout, P. B. *J. Phys. Chem.* **1993**, *97*, 10204−10210.
(68) Rodgers, M. T.; Armentrout, P. B. *J. Phys. Chem. A* **1997**, *101*, 1238−1249.
(69) Armentrout, P. B.; Kickel, B. L. In *Organometallic Ion Chemistry*; Freiser, B. S., Ed.; Kluwer: Dordrecht, 1996; pp 1−45.
(70) Armentrout, P. B.; Simons, J. *J. Am. Chem. Soc.* **1992**, *114*, 8627−8633.
(71) Rodgers, M. T.; Armentrout, P. B. *J. Chem. Phys.* **1998**, *109*, 1787−1800.
(72) Gioumousis, G.; Stevenson, D. P. *J. Chem. Phys.* **1958**, *29*, 294−299.
(73) Sievers, M. R.; Chen, Y.-M.; Armentrout, P. B. *J. Chem. Phys.* **1996**, *105*, 6322−6333.
(74) Zhang, X.-G.; Liyanage, R.; Armentrout, P. B. *J. Am. Chem. Soc.* **2001**, *123*, 5563−5575.
(75) Zhang, X.-G.; Armentrout, P. B. *J. Phys. Chem. A*, accepted for publication.
(76) Chase, M. W.; Davies, C. A.; J. R. Downey, J.; Frurip, D. J.; McDonald, R. A.; Syverud, A. N. *J. Phys. Chem. Ref. Data* **1985**, *14*, Suppl. 1.
(77) Heinemann, C.; Koch, W.; Schwarz, H. *Chem. Phys. Lett.* **1995**, *245*, 509−518.
(78) Sassenberg, U.; Scullman, R. *Physica Scripta* **1983**, *28*, 139.